Automotive Radar Interference Mitigation using Phase-Coded FMCW Waveform

Kumbul, Utku; Petrov, Nikita; Vaucher, Cicero S.; Yarovoy, Alexander

DOI
10.1109/JCS61227.2024.10646233

Publication date
2024

Document Version
Final published version

Published in
2024 IEEE 4th International Symposium on Joint Communications and Sensing, JC and S 2024

Automotive Radar Interference Mitigation Using Phase-Coded FMCW Waveform

Utku Kumbul*†, Nikita Petrov‡†, Cicero S. Vaucher‡†, Alexander Yarovoy†
* IMEC, Eindhoven, The Netherlands
† Department of Microelectronics, Delft University of Technology, Delft, The Netherlands
‡ NXP Semiconductors, Eindhoven, The Netherlands
{utku.kumbul}@imec.nl

2024 IEEE 4th International Symposium on Joint Communications & Sensing (JC&S) | 979-8-3503-8544-1/24/$31.00 ©2024 IEEE | DOI: 10.1109/JCS61227.2024.10646233

***Abstract*—Automotive radar interference problem between multiple radar sensors is investigated. Phase-coded frequency modulated continuous wave (PC-FMCW) radar structure with low sampling and processing power demands is introduced to blindly mitigate mutual interference. The interference resiliency of the proposed structure is evaluated and compared with the conventional frequency modulated continuous wave (FMCW) automotive radar. It is demonstrated that the proposed approach is more robust to both coherent and non-coherent interference types, allowing resilience to both external interference of radars but also the self-interference in the simultaneous multiple input multiple output (MIMO) transmission.**

***Index Terms*—Automotive radar, Interference mitigation, Phase-coded FMCW, Phase coding, Modulated chirps, Mutual interference.**

I. Introduction

Automotive radars widely use linear frequency modulated continuous wave (FMCW), which can offer low sidelobe levels, high range resolution, and good Doppler tolerance using a small analogue bandwidth of the receiver and simple hardware structure [1]. However, the poor distinctness of the FMCW radar makes it vulnerable to mutual interference [2]–[4]. Depending on the spectral characteristic of the interference between FMCW radars, captured interference can be seen as wide-band (WB) or narrow-band (NB) interference [5]. The wide-band interference occurs when the interference has a different chirp slope from the radar being interfered with, known as victim radar. In such an interference scenario, the interference power spreads over multiple range bins and raises the noise floor of the victim radar. The narrow-band interference scenario happens when the interference has the same chirp slope as the victim radar. In this interference scenario, the interference power is concentrated at one particular range bin and leads to a ghost target [6]. Although the ghost target scenario is very difficult to be generated by other radars, the self-interference might cause such a coherent interference scenario seen in the simultaneous multiple-input-multiple-output (MIMO) transmission. Both of these interference types degrade the sensing performance of the automotive radar [6]–[8]. Consequently, many approaches with different costs and computational complexity are studied to mitigate mutual interference [9]–[11]. However, automotive radars have simple hardware and limited processing power, which restricts them from utilizing computationally heavy techniques to mitigate interference. This has motivated the idea of modulating chirp signals with phase-codes jointly in fast-time and slow-time.

978-8-3503-8544-1/24/$31.00 ©2024 IEEE

Lately, phase-coded frequency modulated continuous wave (PC-FMCW) has been investigated to improve mutual orthogonality of the waveforms as well as enable joint sensing and communication [12]–[16]. To decrease the sampling requirements (usually tens of MHz for automotive radar applications), the PC-FMCW waveforms are processed with dechirping followed by the group delay filter and decoding in [15], [16]. However, the dispersion effect (quadratic phase shift) of the group delay filter distorts the received code inside the dechirped signal and causes an imperfection in decoding. Thus, using a code with large code bandwidth (high number of phase changes per chirp) degrades the sensing performance substantially [17]. Such performance degradation limits the code bandwidth and, associated with it, signal isolation. This limitation is circumvented by using phase smoothing and phase lag compensation in [18].

In this paper, we investigate a PC-FMCW radar structure with low sampling and processing requirements for automotive radar interference mitigation. We examine the interference resiliency of the introduced radar structure against both wide-band and narrow-band interference and compare it with the conventional FMCW automotive radar. To achieve this task, we give the signal models for the waveform and mutual interference scenario in Section II. Then, we investigate the processing steps for the proposed architecture in Section III. Subsequently, the sensing performance comparisons of both FMCW and proposed PC-FMCW radar under both wide-band and narrow-band interference are demonstrated in Section IV. Finally, the conclusions are drawn in Section V.

II. System Model

This section introduces the signal model and preliminary study for the proposed PC-FMCW radar structure with low sampling and processing power demands [18]. In the PC-FMCW radar, the phase-coded signal $s(t)$ is used to modulate chirp phases. Thus, the code sequence $s(t)$ controls the phase changes inside a chirp signal (fast-time coding) and a chip duration is defined by $T_c = T/N_c$, where T is the chirp duration and N_c is the number of chips within one chirp. Note that the code bandwidth $B_c = N_c/T$ raises as N_c increases.

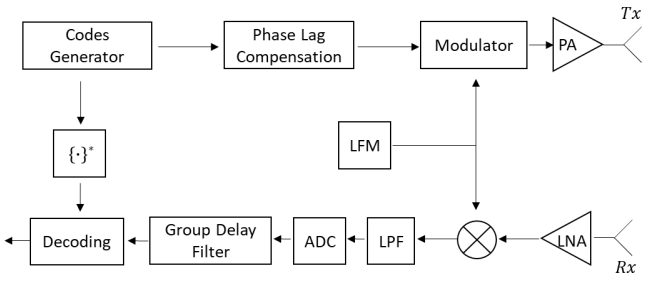

Fig. 1: Block diagram of the proposed PC-FMCW radar structure.

In this study, we consider the chip bandwidth B_c is smaller than the chirp bandwidth B to avoid spectrum leakage.

The block diagram of the proposed PC-FMCW radar structure is illustrated in Fig. 1. The proposed radar structure applies phase lag compensation (PLC) on the phase-coded signal before transmission. Such a filter is required to eliminate the undesired effect of the group delay filter that will be applied in the receiver part. The PLC is equal to a complex conjugate of the group delay filter's frequency response and can be written as:

$$H_{\text{plc}}(f) = e^{-j\left(\frac{\pi f^2}{k}\right)}, \tag{1}$$

where $k = B/T$ is the chirp slope. The spectrum of the transmitted code is multiplied with the PLC filter before transmission as:

$$\hat{s}(t) = \mathcal{F}^{-1}\left\{\mathcal{F}\left\{s(t)\right\} H_{\text{plc}}(f)\right\}, \tag{2}$$

where $\hat{s}(t)$ is the phase-coded signal modified by a PLC filter and $\mathcal{F}\{.\}$ denotes the Fourier transform. Then, the transmitted PC-FMCW waveform of the victim radar can be written as:

$$x_{\text{t}}(t) = \sqrt{P_t}\,\hat{s}(t)e^{-j(2\pi f_c t + \pi k t^2)}, \quad t \in [0, T], \tag{3}$$

where P_t is the transmit signal power and f_c is the carrier frequency of the victim radar. The transmitted signal (3) is reflected from a target and received with a delay. The received PC-FMCW signal can be written as:

$$x_{\text{r}_{\text{tar}}}(t) = \alpha_0\,\hat{s}(t-\tau_0)e^{-j\left(2\pi f_c(t-\tau_0)+\pi k(t-\tau_0)^2\right)}, \tag{4}$$

where τ_0 is the time delay between the victim radar and the target, $\alpha_0 = e^{j\varphi_0}\sqrt{P_{\text{tar}}}$ is the amplitude of received target echo, P_{tar} is the received power of the target echo, and $e^{j\varphi_0}$ is a constant phase term due to two-way propagation of the wave and the scattering coefficient from the target. Assume there is an interfering radar that transmits the FMCW waveform. Then, the received interference can be written as:

$$x_{\text{r}_{\text{int}}}(t) = \alpha_{\text{int}}e^{-j\left(2\pi f_{c\text{i}}(t-\tau_{\text{i}})+\pi k_{\text{int}}(t-\tau_{\text{i}})^2\right)}, \tag{5}$$

where τ_{i} is the time delay between the victim and interfering radars, $\alpha_{\text{int}} = e^{j\varphi_{\text{int}}}\sqrt{P_{\text{int}}}$ is the amplitude of received interference, P_{int} is the received power of the interference signal, $e^{j\varphi_{\text{int}}}$ is a constant phase term due to one-way propagation and the initial phase of the interference, $f_{c\text{i}}$ is the carrier frequency, k_{int} is the chirp slope, B_{int} is the chirp bandwidth and T_{int} is the chirp duration of the interfering radar, respectively. For the derivations, we consider the interference signal overlaps in time with the victim signal. Moreover, the received signal powers P_{tar} and P_{int} can be obtained as:

$$P_{\text{tar}} = \frac{P_t G_t G_r \lambda^2 \sigma}{(4\pi)^3 R^4_{\text{tar}}}, \tag{6}$$

and

$$P_{\text{int}} = \frac{P_{t_{\text{int}}} G_{t_{\text{int}}} G_r \lambda^2{}_{\text{int}}}{(4\pi)^2 R^2_{\text{int}}}. \tag{7}$$

Herein, λ is the wavelength, G_t is the gain of the transmitting antenna, and G_r is the gain of the receiving antenna for the victim radar. Similarly, λ_{int} is the wavelength, $P_{t_{\text{int}}}$ is the transmitting power, and $G_{t_{\text{int}}}$ is the gain of the transmitting antenna for the interfering radar. The σ is the radar cross-section of the target, and R_{tar} and R_{int} are the range of target and interfering radar, respectively. It should be noted that the power of interference is inversely proportional to the interference range, shown as $P_{\text{int}} \propto R_{\text{int}}^{-2}$, while the target echo is inversely proportional to the target range, described as $P_{\text{tar}} \propto R_{\text{tar}}^{-4}$. This may lead to the reception of a strong interference signal that can mask the weak target echoes.

The total received signal in the victim radar is the combination of the target echo and the interference signal. During the dechirping process, the total received signal is mixed with the complex conjugate of the reference transmit signal associated with the victim radar. Then, the resulting beat signal on the victim radar becomes [8], [18]:

$$\begin{aligned} x_{\text{b}}(t) &= \left(x_{\text{r}_{\text{tar}}}(t) + x_{\text{r}_{\text{int}}}(t)\right) e^{j\left(2\pi f_c t + \pi k t^2\right)} \\ &\approx \alpha_0 \hat{s}(t-\tau_0)e^{j(2\pi f_b t)} \\ &+ \alpha_{\text{int}}\, e^{j2\pi\left(f_{c_{\text{i}}}\tau_{\text{i}} + (f_c - f_{c_{\text{i}}} + k_{\text{int}}\tau_{\text{i}})t + (\frac{k-k_{\text{int}}}{2})t^2 - \frac{k_{\text{int}}{\tau_{\text{i}}}^2}{2}\right)} \\ &= x_{\text{b}_{\text{tar}}}(t) + x_{\text{b}_{\text{int}}}(t), \end{aligned} \tag{8}$$

where $f_b = k\tau_0$ is the target beat frequency, the constant phase terms related to target echo substituted into α_0 and we used $(1 - 2v_0/c) \approx 1$ considering that the typical target velocities satisfy $v_0 \ll c$ for automotive radar scenarios. The resulting beat signal has two main components: $x_{\text{b}_{\text{tar}}}(t)$ that contains a delayed phase-coded signal with a single tone beat frequency and $x_{\text{b}_{\text{int}}}(t)$ that contains a signal with quadratic time component due to interference.

III. Signal Processing

This section focuses on the signal processing of the resulting beat signal (8). It should be noted that the resulting beat signal has the delayed phase-coded signal $\hat{s}(t-\tau_0)$ for a particular target. Thus, the phase-coded beat signals from all ranges need to be aligned in the fast-time before performing decoding with the reference code. Such an alignment in the fast-time can be employed with the group delay filter that causes a group delay $\tau_g(f)$ [18]. The group delay corresponds to the first

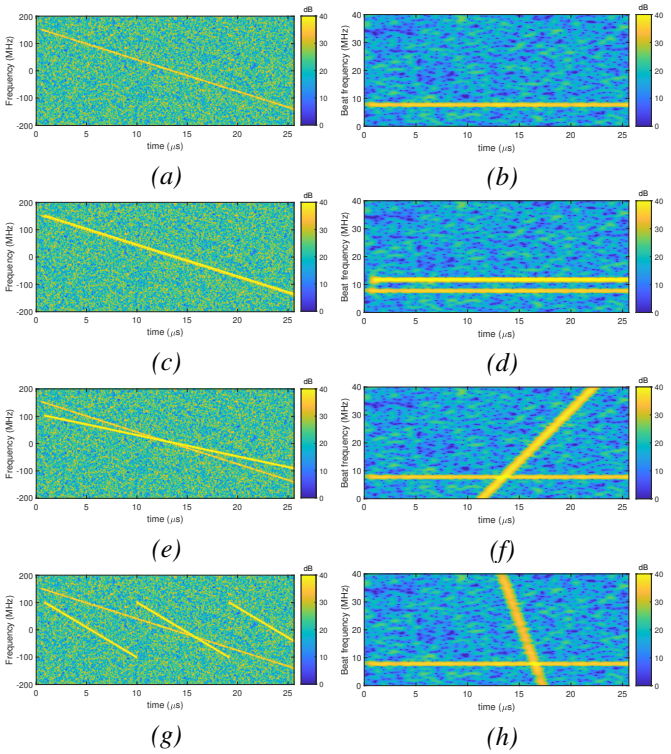

Fig. 2: Spectrogram of the FMCW victim radar with different interference scenarios. The received signal on the left column and the dechirped signal on the right column: (a)-(b) No interference (c)-(d) Coherent NB interference (e)-(f) Coherent WB interference (g)-(h) Non-coherent WB interference.

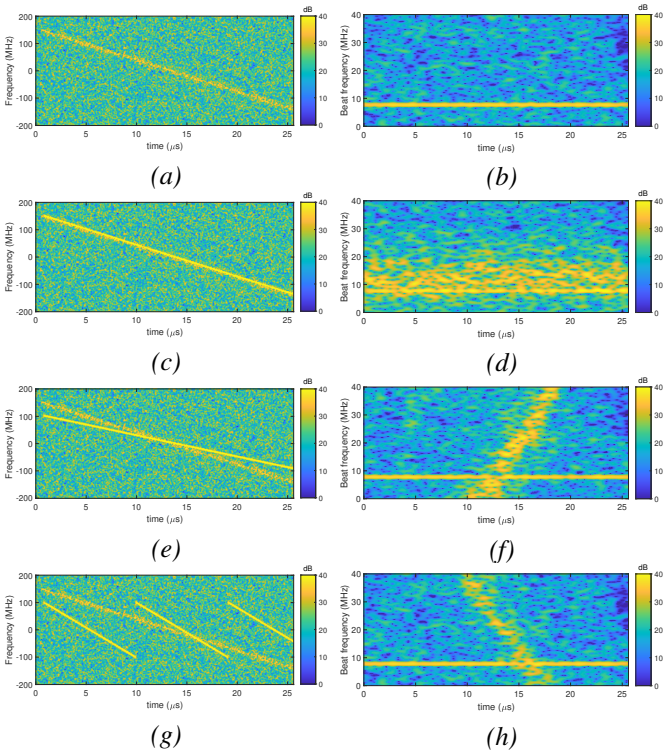

Fig. 3: Spectrogram of the PC-FMCW victim radar ($N_c = 1024$) with different interference scenarios. The received signal on the left column and the decoded dechirped signal on the right column: (a)-(b) No interference (c)-(d) Coherent NB interference (e)-(f) Coherent WB interference (g)-(h) Non-coherent WB interference.

derivative of the filter phase response and shifts the envelope of the signal. To eliminate τ_0 and align coded beat signals, the desired group delay can be represented as:

$$\tau_{\mathrm{g}}(f) = -\frac{1}{2\pi}\frac{d\theta(f)}{df}\bigg|_{f=f_b} = -\tau_0 = -f_b/k. \tag{9}$$

Then, the desired group delay filter's frequency response can be given as:

$$H_{\mathrm{g}}(f) = e^{j\left(\frac{\pi f^2}{k}\right)}. \tag{10}$$

We apply the resulting group delay filter to the spectrum of the beat signal (8). As a result, each coded beat signal is perfectly aligned with the help of phase lag compensation, and the delay τ_0 inside the phase-code signal is eliminated for each target [18]. Subsequently, we perform decoding by multiplying the resulting time-domain signal with the complex conjugate of the reference code and take fast Fourier Transform (FFT) for the range processing as:

$$y_o(\tau) = \mathcal{F}\left\{\mathcal{F}^{-1}\left\{\mathcal{F}\left\{x_{\mathrm{b}}(t)\right\} H_{\mathrm{g}}(f)\right\} s^*(t)\right\}, \tag{11}$$

where the outer FFT corresponds to the range processing after decoding. Herein, the beat signal reflected from the target is obtained similar to the dechirped signal of conventional FMCW. Thus, the proposed structure allows to processing of the PC-FMCW signal with a low sampling (typically tens of MHz) and utilization of FFT-based processing instead of full-band matched filtering. Moreover, it should be noted that the beat signal initiated by the interfering radar remains coded [18]. The phase-coded signal spreads the peak power of the signals in the beat frequency domain. Since each transmitted PC-FMCW chirp pulse utilizes a different (ideally orthogonal) phase-coded signal, only the correct signal matched to this code will be decoded. The interfering signals without code (FMCW) or with other code sequences (PC-FMCW) that are not matched to this code remain coded, causing the spread of the interference peak power over range domain with fast-time coding and over Doppler domain combining it with slow-time coding. This allows to suppression of the interference signals blindly and separates the self-transmitted signal from the interference. Consequently, the proposed PC-FMCW structure can be used to blindly mitigate the mutual interference between multiple radars and also the self-interference between multiple transmitters in the coherent MIMO radar [14].

IV. Performance Assessment

This section investigates the radar-to-radar interference resilience of the proposed PC-FMCW radar. To this end, we consider different FMCW interference scenarios and compare their impact on the sensing performance of both FMCW and

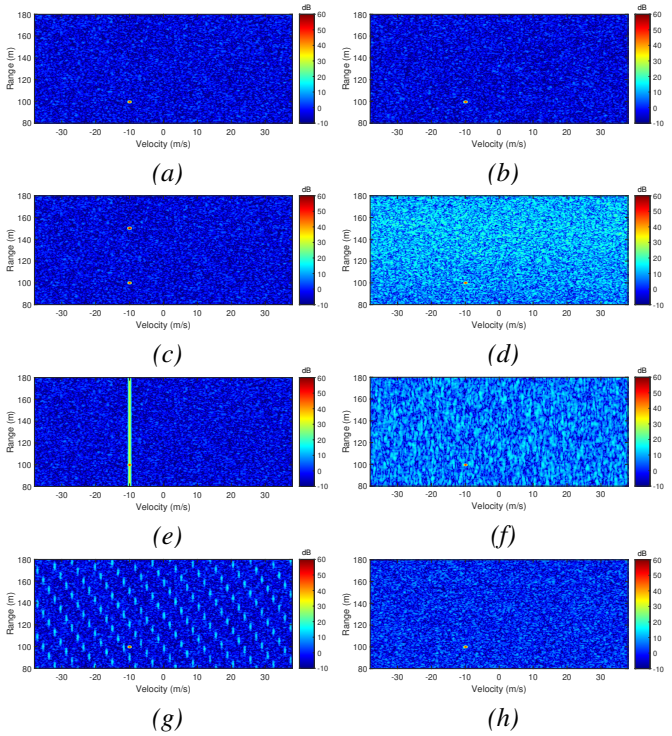

Fig. 4: Comparison of range-Doppler profiles. The FMCW victim radar on the left column and the PC-FMCW victim radar ($N_c = 1024$, $N_p = 256$) on the right column: (a)-(b) No interference (c)-(d) Coherent NB interference (e)-(f) Coherent WB interference (g)-(h) Non-coherent WB interference.

PC-FMCW victim radars. Assume the FMCW and PC-FMCW victim radars operate at carrier frequency $f_c = 77$ GHz and transmit $N_p = 256$ chirp pulses with a chirp bandwidth $B = 300$ MHz and a chirp duration $T = 25.6$ μs. Each chirp signal is modulated with a phase-coded signal in both fast-time and slow-time for the PC-FMCW victim radar. In this study, we employ random code sequences with Gaussian Minimum Shift Keying (GMSK) coding scheme for the phase-coded signal $s(t)$, and apply the phase lag compensation before transmitting the code. We use $N_c = 1024$ number of chips per chirp for fast-time coding, i.e. the code bandwidth becomes $B_c = 40$ MHz with $N_c = 1024$ for this setting. Moreover, each chirp pulse utilizes different phase lag compensated code signal $\hat{s}(t)$ for slow-time coding. For the numerical simulations, we also assume a complex Gaussian noise signal with power spectral density N_0 is captured along with the received signal. The signal-to-noise ratio (SNR) can be defined as SNR $= {\alpha_0}^2/N_0$. We give the noise signal power N_0 relative to the absolute of α_0 and set SNR $= -10$ dB. Moreover, we consider all chirp pulses of victim radar are interfered with the FMCW interference radar operating at carrier frequency $f_{c_\text{i}} = 77$ GHz. We set the received interference signal power 6 dB higher than the victim radar signal power.

The captured interference might appear as the NB or WB interference based on the spectral characteristics of the interference [5]. We simulate three different interference scenarios to investigate their effects. The first one is the fully coherent NB interference by letting $T_\text{int} = 25.6$ μs and $B_\text{int} = 300$ MHz. The second one is the coherent WB interference by letting $T_\text{int} = 25.6$ μs and $B_\text{int} = 200$ MHz. Finally, the third one is the non-coherent WB interference by letting $T_\text{int} = 9$ μs and $B_\text{int} = 200$ MHz. For all cases, we assume the interference radar is located at a range $R_\text{int} = 300$ m with a radial velocity $v_\text{int} = -20$ m/s, and the target is located at the range $R = 100$ m with a radial velocity $v = -10$ m/s. On the receiver side, the total received signal is dechirped with the reference chirp signal of victim radar. Then, the dechirped signal is sampled with $f_s = 80$ MHz and low-pass filtered (LPF) with the cut-off frequency $f_\text{cut} = \pm 40$ MHz. Consequently, we have $N = 2048$ range cells (fast-time samples) for the selected parameters. In the case of PC-FMCW victim radar, the group delay filter is applied to the sampled signal. The same LPF is applied to the reference phase-coded signal to prevent a signal mismatch, and then the decoding is performed. We apply 80 dB Chebyshev window in the range domain, and 60 dB Chebyshev window in the Doppler domain, before taking the two-dimensional FFT. In addition, we normalize the range-Doppler profiles with respect to the noise level to focus on the impact of interference.

First, we illustrate the spectrogram of the FMCW victim radar with different FMCW interference cases in Figure 2. It can be seen that the received target echo creates a single tone beat signal in the dechirped signal in no interference case. Note that the noise peak power is decreased after stretch processing (dechirping) and low-pass filtering. The suppression of the peak noise power after taking FFT is $10\log_{10}(BT) = 38$ dB for a single chirp and an additional $10\log_{10}(N_p) = 24$ dB after coherent pulse integration for Doppler processing. In case of the interference has the same chirp slope and chirp duration, i.e. $k_\text{int} = k$ and $T_\text{int} = T$, the coherent NB interference scenario occurs, and the received interference causes another single tone beat signal in the dechirped signal (Figure 2 d). In case of the interference has the same chirp duration but has a different chirp slope $k_\text{int} \neq k$, the coherent WB interference scenario occurs, and the received interference causes a diagonal line for the complex mixer as shown Figure 2 f. Such interference will create "V-shape" in the spectrogram for the real mixer as discussed in [4]. It is important to note that coherent interference scenarios create the same effect for each chirp pulse. In case of the interference has different chirp duration $T_\text{int} \neq T$ and chirp slope $k_\text{int} \neq k$, the non-coherent WB interference scenario occurs, and the received interference causes different impact for each chirp pulse. The spectrogram of the dechirped signal with non-coherent WB interference is shown for the first pulse in 2 h. For comparison, we demonstrate the spectrogram of the PC-FMCW victim radar with $N_c = 1024$ against investigated interference scenarios in Figure 3. We observe that the self-transmitted signal (signal reflected from the target) is perfectly decoded, and a single tone beat signal associated with the target is recovered after applying the group delay filter and decoding as explained in Section III. On the other hand, all

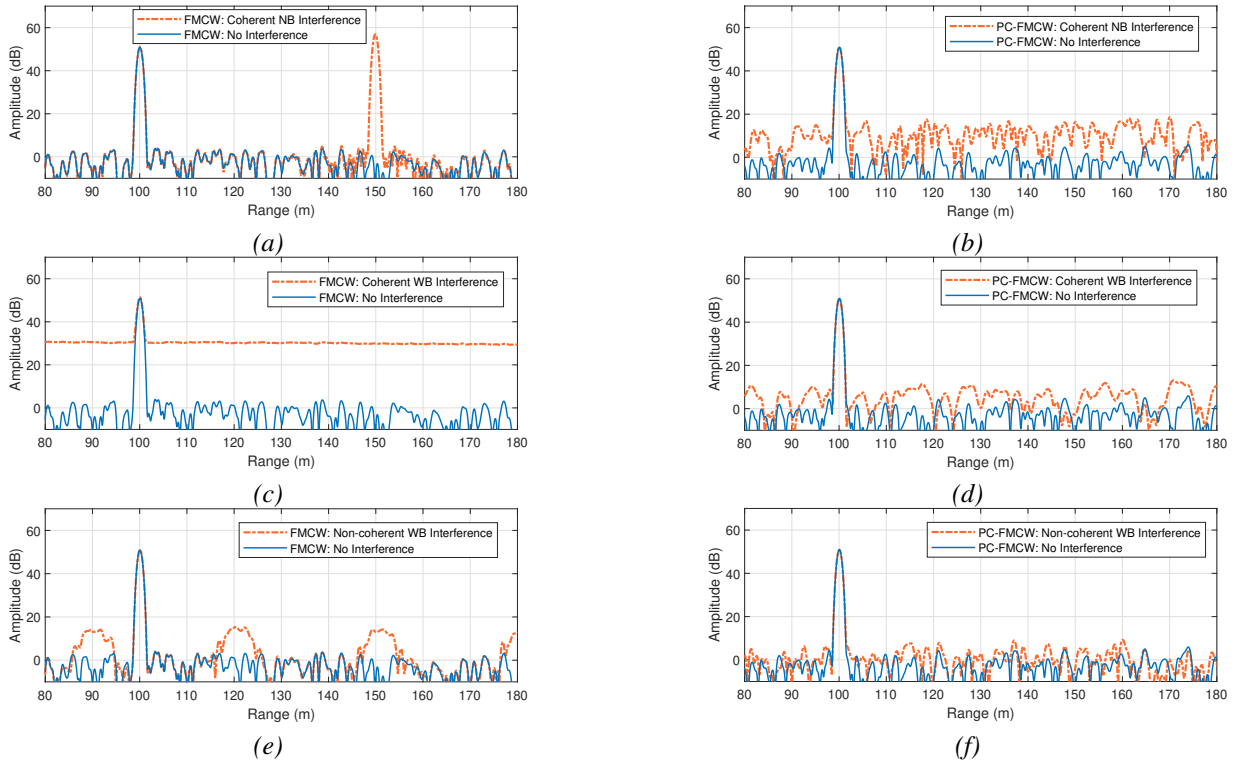

Fig. 5: Comparison of range profiles. The FMCW victim radar on the left column and the PC-FMCW victim radar on the right column: (a)-(b) Coherent NB interference (c)-(d) Coherent WB interference (e)-(f) Non-coherent WB interference.

other interference signals remain coded, and thus their peak powers are spread over fast-time for each chirp pulse. This enables the suppression and isolation of interference signals. Notice that the suppression performance is proportional to the code bandwidth $B_c = N_c/T$ as the spectrum spread with the time-bandwidth product. Thus, the suppression performance improves as we increase the number of chips per chirp and can be written as $10\log_{10}(N_c)$ for a single chirp.

Next, we examine the range-Doppler profiles of the FMCW and PC-FMCW victim radars in Figure 4, and we compare their range profiles in Figure 5. In the interference-free case, both radars have the target response with ~ 51 dB dynamic range at 100 m with a -10 m/s radial velocity. In the coherent NB interference case, the interference peak power concentrates at one particular range bin and leads to a ghost target at 150 m with a -10 m/s radial velocity for the FMCW victim radar (Figure 4 c). The resulting ghost target has ~ 57 dB power as seen in Figure 5 a. This ghost target can not be distinguished from the real target and hence needs to be mitigated. Notice that the ghost target scenario is very difficult to be generated by other radars as the interference radar should be fully synchronized with the victim radar. On the other hand, such a coherent interference case can mimic a self-interference scenario, which is the interference case seen in the simultaneous MIMO transmission [14]. As shown in Figure 4 d, the PC-FMCW victim radar spread the peak power of such an interference over the range-Doppler plane using both fast-time and slow-time coding. Thus, the peak power of the ghost target is expected to be suppressed $10\log_{10}(N_c) + 10\log_{10}(N_p) = 54$ dB on average for the perfectly orthogonal codes. In Figure 5 b, we observe that the ghost target peak power is decreased and has a noise-like pattern with a maximum of 18 dB. In the case of coherent WB interference, the interference peak power starts to spread over multiple range bins and increases the noise floor in the range profile of the FMCW victim radar (Figure 4 e). However, this interference type affects only the range profile, since the interference is coherent over Doppler processing. In this particular example, we observe that the noise floor of the FMCW victim radar raised from 0 dB to ~ 30 dB as shown in Figure 5 c. On the other hand, the PC-FMCW victim radar further suppresses the coherent WB interference and decreases the noise floor due to interference to ~ 10 dB (Figure 5 d). In the case of non-coherent WB interference, the interference peak power starts to spread over both multiple range and Doppler cells of the FMCW victim radar (Figure 4 g). It is important to note that the non-coherent WB interference already has a noise-like pattern as it spans multiple range-Doppler cells, and hence the interference peak power is already spread. For this setting, we observe that such an interference causes responses periodically every 30 m with ~ 15 dB power (Figure 5 e). By utilizing phase-coding in both slow-time and fast-time, the PC-FMCW victim radar further spreads such an interference over the whole range-Doppler profile, and the peak power of this interference is reduced to ~ 8 dB as shown

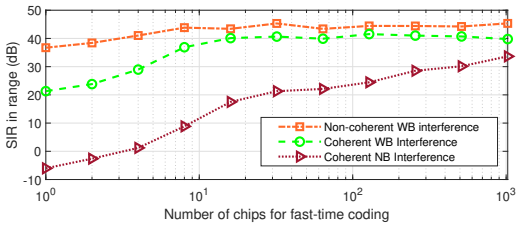

Fig. 6: SIR in range versus the number of chips for fast-time coding of the PC-FMCW victim radar.

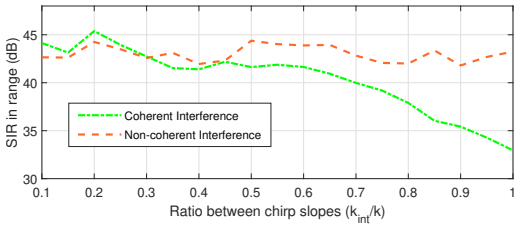

Fig. 7: SIR in range versus the ratio between chirp slopes (k_{int}/k) of the PC-FMCW victim radar.

in Figure 5 f. Therefore, the PC-FMCW waveforms can be used to mitigate both NB and WB interference types.

Finally, we demonstrate signal-to-interference ratio (SIR) in range as a function number of chips for fast-time coding of the PC-FMCW victim radar in Figure 6, and assess the interference resilience of the PC-FMCW radar against different interference types. It should be noted that the PC-FMCW victim radar also utilizes $N_p = 256$ chirp pulses for slow-time coding. As the number of chips for fast-time coding is increased from $N_c = 0$ to $N_c = 1024$, we observe that the SIR in range is improved from -6 dB to 33 dB for the coherent NB interference, 21 dB to 39 dB for the coherent WB interference, and 36 dB to 45 dB for the non-coherent WB interference. In addition, we illustrate the SIR in range versus the ratio between chirp slopes in Figure 7. Herein, we use $N_c = 1024$ and $N_p = 256$ for the PC-FMCW victim radar. Moreover, we set $T_{\text{int}} = 25.6$ μs for coherent and $T_{\text{int}} = 9$ μs for non-coherent interference types and then change the interference chirp bandwidth B_{int} to investigate different chirp slope ratio. It can be seen that the SIR in range is around $\sim$ 43 dB for different chirp slope values in the non-coherent interference case as shown in Figure 7. However, SIR in range changes from 45 dB to 33 dB as the ratio k_{int}/k raises from 0.1 to 1. This is because the WB interference becomes NB that causes the ghost target case as the ratio k_{int}/k approaches 1.

V. Conclusion

The automotive radar interference problem has been investigated. A PC-FMCW radar structure with low sampling and processing demands has been proposed to blindly mitigate automotive radar interference. The sensing performance of the introduced structure is compared with the conventional FMCW automotive radar under coherent NB, coherent WB and non-coherent WB interference cases. We show that the developed PC-FMCW radar spreads the peak power of the interference signal over the range-Doppler profile by combining phase coding in both fast-time and slow-time. Thus, it is demonstrated that the PC-FMCW radar improves the SIR in range profile compared to the FMCW radar case. Consequently, mutual interference between multiple automotive radars and the self-interference between coherent MIMO transmission can be mitigated by using the proposed approach.

References

[1] I. Bilik, O. Longman, S. Villeval, and J. Tabrikian, "The rise of radar for autonomous vehicles: Signal processing solutions and future research directions," *IEEE Signal Process. Mag.*, vol. 36, no. 5, pp. 20–31, Sep. 2019.

[2] G. M. Brooker, "Mutual interference of millimeter-wave radar systems," *IEEE Transactions on Electromagnetic Compatibility*, vol. 49, no. 1, pp. 170–181, 2007.

[3] T. Schipper, S. Prophet, M. Harter, L. Zwirello, and T. Zwick, "Simulative prediction of the interference potential between radars in common road scenarios," *IEEE Transactions on Electromagnetic Compatibility*, vol. 57, no. 3, pp. 322–328, 2015.

[4] U. Kumbul, F. Uysal, C. S. Vaucher, and A. Yarovoy, "Automotive radar interference study for different radar waveform types," *IET Radar, Sonar Navigation*, vol. 16, no. 3, pp. 564–577, 2022. [Online]. Available: https://ietresearch.onlinelibrary.wiley.com/doi/abs/10.1049/rsn2.12203

[5] S. Alland, W. Stark, M. Ali, and M. Hegde, "Interference in automotive radar systems: Characteristics, mitigation techniques, and current and future research," *IEEE Signal Process. Mag.*, vol. 36, no. 5, pp. 45–59, Sep. 2019.

[6] M. Goppelt, H. . Blöcher, and W. Menzel, "Analytical investigation of mutual interference between automotive fmcw radar sensors," in *2011 German Microwave Conference*, 2011, pp. 1–4.

[7] A. Al-Hourani, R. J. Evans, S. Kandeepan, B. Moran, and H. Eltom, "Stochastic geometry methods for modeling automotive radar interference," *IEEE Transactions on Intelligent Transportation Systems*, vol. 19, no. 2, pp. 333–344, 2018.

[8] U. Kumbul, Y. Chen, N. Petrov, C. S. Vaucher, and A. Yarovoy, "Impacts of mutual interference analysis in fmcw automotive radar," in *2023 17th European Conference on Antennas and Propagation (EuCAP)*, 2023, pp. 1–5.

[9] M. Kunert, H. Meinel, C. Fischer, and M. Ahrholdt, "Report on interference density increase by market penetration forecast," in *MOSARIM Consortium, CNTR, Tech. Rep. D1.6, Sep.*, 2010.

[10] A. Bourdoux and M. Bauduin, "PMCW waveform cross-correlation characterization and interference mitigation," in *Proc. 17th Eur. Radar Conf.*, Jan. 2021, pp. 164–167.

[11] F. Roos, J. Bechter, C. Knill, B. Schweizer, and C. Waldschmidt, "Radar sensors for autonomous driving: Modulation schemes and interference mitigation," *IEEE Microw. Mag.*, vol. 20, no. 9, pp. 58–72, Sep. 2019.

[12] P. M. McCormick, C. Sahin, S. D. Blunt, and J. G. Metcalf, "FMCW implementation of phase-attached radar-communications (PARC)," in *Proc. IEEE Radar Conf.*, Apr. 2019, pp. 1–6.

[13] U. Kumbul, N. Petrov, C. S. Vaucher, and A. Yarovoy, "Performance analysis of phase-coded fmcw for joint sensing and communication," in *2023 24th International Radar Symposium (IRS)*, 2023, pp. 1–10.

[14] U. Kumbul, N. Petrov, C. S. Vaucher, and A. Yarovoy, "Phase-coded fmcw for coherent mimo radar," *IEEE Transactions on Microwave Theory and Techniques*, vol. 71, no. 6, pp. 2721–2733, 2023.

[15] F. Lampel, R. F. Tigrek, A. Alvarado, and F. M. J. Willems, "A performance enhancement technique for a joint FMCW radcom system," in *Proc. 16th Eur. Radar Conf.*, Oct. 2019, pp. 169–172.

[16] F. Uysal, "Phase-coded FMCW automotive radar: System design and interference mitigation," *IEEE Trans. Veh. Technol.*, vol. 69, no. 1, pp. 270–281, Jan. 2020.

[17] U. Kumbul, N. Petrov, C. S. Vaucher, and A. Yarovoy, "Receiver structures for phase modulated FMCW radars," in *Proc. 16th Eur. Conf. Antennas Propag.*, Mar. 2022, pp. 1–5.

[18] U. Kumbul, N. Petrov, C. S. Vaucher, and A. Yarovoy, "Smoothed phase-coded fmcw: Waveform properties and transceiver architecture," *IEEE Transactions on Aerospace and Electronic Systems*, vol. 59, no. 2, pp. 1720–1737, 2023.